AIAA SciTech Forum
January 3-7, 2022, San Diego, CA & Virtual
AIAA SCITECH 2022 Forum

10.2514/6.2022-2234

Check for updates

Supersonic Axis-symmetric Mixed-Compression Inlet Using Zero-Net-Mass-Flux CoFlow Jet Flow Control

Zhijin Lei*, Yan Ren†, Gecheng Zha‡
Dept. of Mechanical and Aerospace Engineering
University of Miami, Coral Gables, Florida 33124
E-mail: gzha@miami.edu

Downloaded by Gecheng Zha on January 3, 2022 | http://arc.aiaa.org | DOI: 10.2514/6.2022-2234

Abstract

This paper numerically studies a new zero-net-mass-flux (ZNMF) coflow jet (CFJ) active control to increase the unstart margin and efficiency of axis-symmetric mixed-compression supersonic inlets without dumping the bleed flow. The simulation is done by using the in-house CFD code FASIP that solves 3D Reynolds-averaged Navier-Stokes (RANS) equations with 3rd order MUSCL scheme for shock capturing, 2nd order central differencing for the viscous terms, and the Spalart-Allmaras model for turbulence. The CFD simulation is validated with the tested NASA VDC Inlet at Mach 2.0 for its critical condition at angle of attack (AoA) of 0°. Good agreement between the CFD simulation and experiment at critical condition is achieved for the streamwise surface pressure distribution, total pressure profiles at different streamwise locations, total pressure recovery, and fan face distortion. The CFD simulation indicates that the baseline inlet remains started at AoA of 1.2° and unstarts at AoA of 1.6°.

A CFJ inlet concept is studied to improve the baseline inlet performance. The CFJ flow control withdraws the mass flow of boundary layer at the same throat position as conventional bleed, but injects the mass flow back to the inlet diffuser area downstream. It thus has a constant mass flow from the supersonic inlet entrance to the engine entrance similar to subsonic inlets. The mechanism of CFJ active flow control to stabilize axis-symmetric inlet is two-fold: i) The suction in the throat bleed region has the same effect as conventional bleed to remove the thick boundary layer and increase flow passing capacity. ii) The downstream injection further energizes the boundary layer in the diffuser region to reduce flow blockage, increases flow passing capacity, and increases inlet stability against unstart. With a 5% less bleed flow than that of the baseline inlet, the CFJ inlet is able to stabilize the inlet at AoA of 2° with higher inlet stability and total pressure recovery, while keeping the constant mass flow in the inlet. More numerical studies to investigate the working mechanism of CFJ inlets are in progress.

Nomenclature

CFJ	Co-flow Jet
AoA	Angle of Attack
M	Mach Number
P_tR	Total Pressure Ratio
U	Flow Velocity
M	Mach Number

* Ph.D. Candidate
† Ph.D. Post Doc Researcher
‡ Professor, ASME Fellow, AIAA associate Fellow

Copyright © 2022 by All authors of this paper. Published by the American Institute of Aeronautics and Astronautics, Inc., with permission.

P	Static Pressure
P_t	Total Pressure
T_t	Total Temperature
P_{pump}	Pumping Power
P_c	Power Coefficient
R_c	Inlet Cowl Lip Radius
P_tR	Total Pressure Recovery
S_{ref}	Reference Area, $= 0.5\pi R_c^2$
l_{ref}	Reference Length, $= R_c$
C_μ	Jet Momentum Coefficient $\dot{m}_j\, U_j/(q_\infty\, S_{ref})$
$\dot{m}$	Bleed Mass Flow Rate
$\dot{m}_0$	Captured Mass Flow Rate
MFR	Mass Flow Ratio, $= \dot{m}/\dot{m}_0$
q	Dynamic Pressure, $= 0.5\,\rho\, U^2$
$\overline{P}$	Mass-averaged Static Pressure
$\overline{P_t}$	Mass-averaged Total Pressure
H	Local Cowl radius, measured in R_cs
x	Location in Axial Direction(Streamwise), measured in R_cs
h	Distance from Centerbody
d	Steady State Distortion, $P_{t,max} - P_{t,min})/\overline{P_t}$
l_{duct}	Slot Width
γ	Specific Heat Ratio
η	Pump Efficiency
ρ	Air Density
∞	Free Stream Conditions
$_j$	Jet Value
$_{max}$	Maximum Value
$_{min}$	Minimum Value
$_{mass-av}$	Mass Average Value
$_{inj}$	Value at Injection slot
$_{suc}$	Value at Suction slot
$_{exit}$	Value at Inlet Exit or Fan Face

Downloaded by Gecheng Zha on January 3, 2022 | http://arc.aiaa.org | DOI: 10.2514/6.2022-2234

1 Introduction

The development of supersonic civil transport (SST) [1, 2, 3] has many challenges such as sonic boom and efficiency. An important component of the propulsion system that affects the whole aircraft efficiency and performance is the supersonic engine inlet, which plays the role to slow down the flow from supersonic to subsonic before entering the core engine. An engine inlet needs to have high efficiency, good flow uniformity and wide stability margin. These performances are measured by total pressure recovery, fan interface (inlet exit) distortion, and inlet stability margin with no unstart to tolerate various disturbances such as variation of angle of attack (AoA), gust, compressor perturbations, etc. To have high inlet efficiency, the desirable position for the terminal normal shock is to be located in the throat region to maintain a low Mach number.

To acquire high stability margin, the normal shock should be positioned downstream of the throat. However,

such a position with high stability margin may suffer severe total pressure loss due to high Mach number in front of the normal shock. If the normal shock is located in the throat region, the inlet is termed at critical condition. If the shock is downstream of the throat, the inlet is termed at supercritical condition. If the shock is pushed outside of the inlet entrance, the inlet is termed at subcritical condition and is unstarted. The inlet at critical and supercritical condition has the normal shock inside the inlet and is termed inlet started. A started inlet has the maximum flow capacity to supply the mass flow needed by the engine.

Supersonic inlets in general have two types based on their cross section shapes: axis-symmetric and rectangular. Axis-symmetric inlets have an advantage over rectangular inlets for their lighter weight as they can directly match the engine interfaces. However, supersonic axis-symmetric inlets have a critical drawback that they in general have smaller stability margin than the rectangular ones and are prone to unstart. Inlet unstart is usually caused by the shock boundary layer interaction that thickens the boundary layer or creates flow separation, which increases the inlet blockage, reduces the flow passing capacity, pushes the normal shock to outside of the inlet entrance and spills the flow. An inlet unstart would result in transient forces on the aircraft, affect passenger comfort and safety. Because of the inlet unstart issues, axis-symmetric inlets are mostly used for military aircraft (e.g. SR-71) or weaponry (e.g. missiles inlets). For supersonic civil transports, rectangular inlets are mostly used (e.g., Concorde, Tu-144) as safety has the dominant priority.

Downloaded by Gecheng Zha on January 3, 2022 | http://arc.aiaa.org | DOI: 10.2514/6.2022-2234

The conventional technique to increase inlet unstart margin for critical condition is to employ a centerbody bleed at the throat, which removes the boundary layer and the blockage to increase the flow capacity. In case the inlet is unstarted, a downstream bypass door on the inlet cowl may be opened to further increase the flow capacity and sallow the shock into the throat area to establish the stable condition. The mass flow removed by bleed and bypass doors is typically discarded to ambient or used for other purpose outside of the engine system. Different from the supersonic counterpart, a subsonic inlet has a constant mass flow rate throughout the system from the inlet entrance to the nozzle exit (neglect the fuel mass flow and secondary flow).

It is beneficial if a supersonic transport engine inlet can be designed with constant mass flow with no bleed flow to be discarded. A constant mass flow brings these important advantages: 1) the core engine can be designed with narrower flow range to provide higher efficiency and wider stall margin. 2) The system efficiency will be substantially increased without discarding the bleed flow energized by the engines. 3) The propulsion system weight can be reduced with smaller captured area and mass flow. 4) The smaller captured area of inlet will also reduce the aircraft drag.

The purpose of the present work is to usher a new active flow control concept that achieves constant mass flow in the inlet with no mass flow discarded as conventional inlet bleed. By energizing and re-injecting 100% of the centerbody bleed flow into the downstream diffuser of the inlet, a zero mass flow loss will be achieved. It means that the mass flow captured by the inlet is the mass flow captured by the core engine. However, a necessary condition of the new flow control method is that the inlet unstart margin must not be sacrificed. It appears that the zero-net-mass-flux co-flow jet active flow control originally developed for airfoil can fulfil this duty.

1.1 Co-Flow Jet (CFJ) Active Flow Control

The CFJ recently developed by Zha *et al*[4, 5, 6, 7, 8, 9, 10, 11, 12, 13, 14, 15] is demonstrated to achieve large lift augmentation, stall margin increase, drag reduction and moderate nose-down moment for stationary and pitching airfoils. In a CFJ airfoil, an injection slot near the leading edge (LE) and a suction slot near the trailing edge on the airfoil suction surface are created. As shown in Fig. 1, a small amount of mass flow is drawn into the suction duct, pressurized and energized by micro compressor actuators, and then injected near the LE tangentially to the main flow via an injection slot. The whole process does not add or dispose any mass flow inside the system

and hence is a zero-net-mass-flux(ZNMF) flow control.

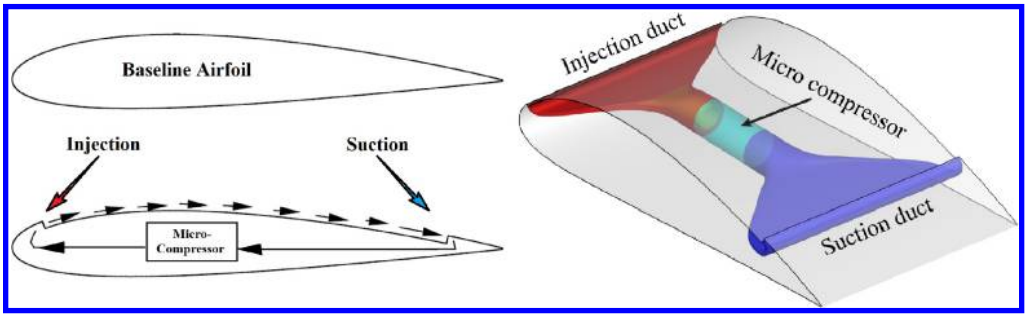

Figure 1: Schematic plot of a typical CFJ airfoil.

Downloaded by Gecheng Zha on January 3, 2022 | http://arc.aiaa.org | DOI: 10.2514/6.2022-2234

The jet momentum coefficient C_μ is a parameter used to quantify the jet intensity. It is defined as:

$$C_\mu = \frac{\dot{m}U_j}{\frac{1}{2}\rho_\infty {U_\infty}^2 S_{ref}} \tag{1}$$

where $\dot{m}$ is the injection mass flow, V_j is the mass-averaged injection velocity, ρ_∞ and V_∞ denote the free stream density and velocity, and S_{ref} is the reference area based on captured area determined by the cowl lip diameter.

The power consumption is determined by the jet mass flow and total enthalpy change as the following:

$$P = \dot{m}(H_{t1} - H_{t2}) \tag{2}$$

where H_{t1} and H_{t2} are the mass-averaged total enthalpy in the injection cavity and suction cavity respectively, P is the power required by the micro-compressor actuators and $\dot{m}$ the jet mass flow rate.

The total power can be expressed with the pump efficiency η and total pressure ratio of the pump $\Gamma = \frac{P_{t1}}{P_{t2}}$ as:

$$P = \frac{\dot{m}C_p T_{t2}}{\eta}(\Gamma^{\frac{\gamma-1}{\gamma}} - 1) \tag{3}$$

where γ is the specific heat ratio equal to 1.4 for air, the power coefficient is expressed as:

$$P_c = \frac{P}{\frac{1}{2}\rho_\infty V_\infty^3 S_{ref}} \tag{4}$$

2 Numerical Algorithms

The in-house high order CFD code Flow-Acoustics-Structure Interaction Package (FASIP) is used to solve the 3D Reynolds averaged Navier-Stokes (RANS) equations. A 3rd order MUSCL scheme for the inviscid flux [16, 17, 18, 19, 20, 21] and 2nd order central differencing for the viscous terms [17, 19] are employed to discretize the Navier-Stokes equations. An implicit time marching with Gauss-Seidel line relaxation is used to achieve

a fast convergence rate [20, 23]. Parallel computing with domain partitioning is implemented for the body-fitted structured mesh to save wall clock simulation time [24]. The FASIP code is intensively validated for CFJ simulations and many steady and unsteady flows [6, 7, 9, 15, 25, 26, 27, 28, 29, 24, 30, 31].

To achieve zero-net mass-flux with the CFJ flow control, the injection mass flow must be equal to the mass flow entering the suction slot. For the supersonic inlet study, a uniform mass flow suction boundary condition used by Zha *et al* [32, 33] is adopted to specify the bleed mass flow. The injection total pressure is iterated to match the same mass flow rate of the suction.

3 Validation

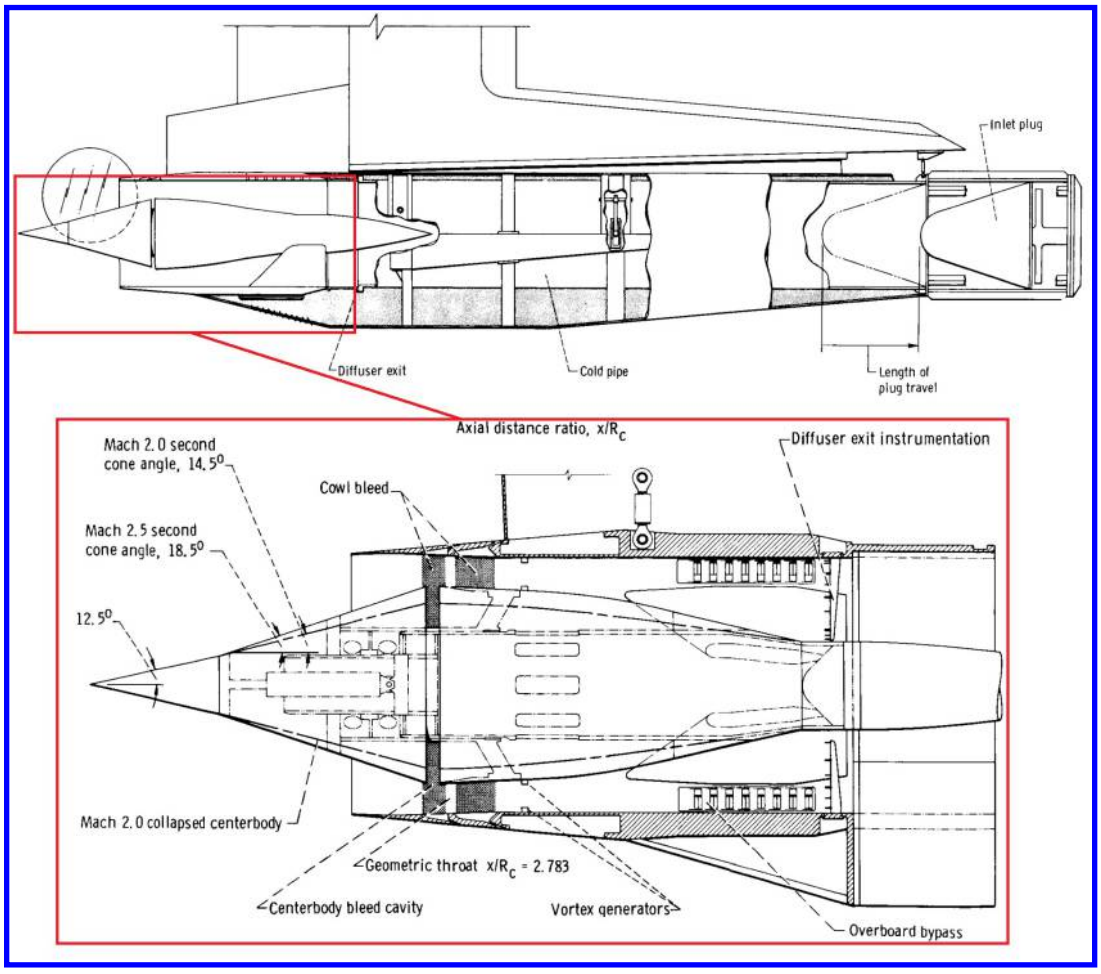

Figure 2: NASA VDC Inlet geometry and cross section, from [34].

The NASA variable diameter centerbody (VDC) supersonic inlet designed by Wasserbauer, *et al* [34, 35], as shown in Fig. 2 attached to a Pratt and Whitney TF30-P-3 engine, which is an axis-symmitric mixed-compression inlet with a 45% internal compression, is used as the baseline for CFD validation. The inlet was tested in the 10- by 10- Foot Supersonic Wind Tunnel of NASA Lewis Research Center in 1975 over a Mach number range from 2.0 to 2.5. Two centerbodies were designed by Wasserbauer *et al* [35], as shown in Fig. 2. The model with Mach 2.0 centerbody is used as the baseline in the present work. Since a steady state flow would be symmetric about

Downloaded by Gecheng Zha on January 3, 2022 | http://arc.aiaa.org | DOI: 10.2514/6.2022-2234

the meridional plane, only half of the inlet is simulated to save CPU time.

A mesh independent study is conducted with a mesh size range between 450,635 and 3,837,600 cells. The final 3-D mesh with a total size of 706,668 cells is adopted and is shown in Fig. 3. The mesh is constructed using O-mesh topology, with 365 points distributed in the streamwise direction, 32 points in the circumferential direction, and 61 points in the radial direction. The cutaway views of the freestream($A-A$), throat($B-B$), and inlet exit ($C-C$) are shown in Fig. 3.

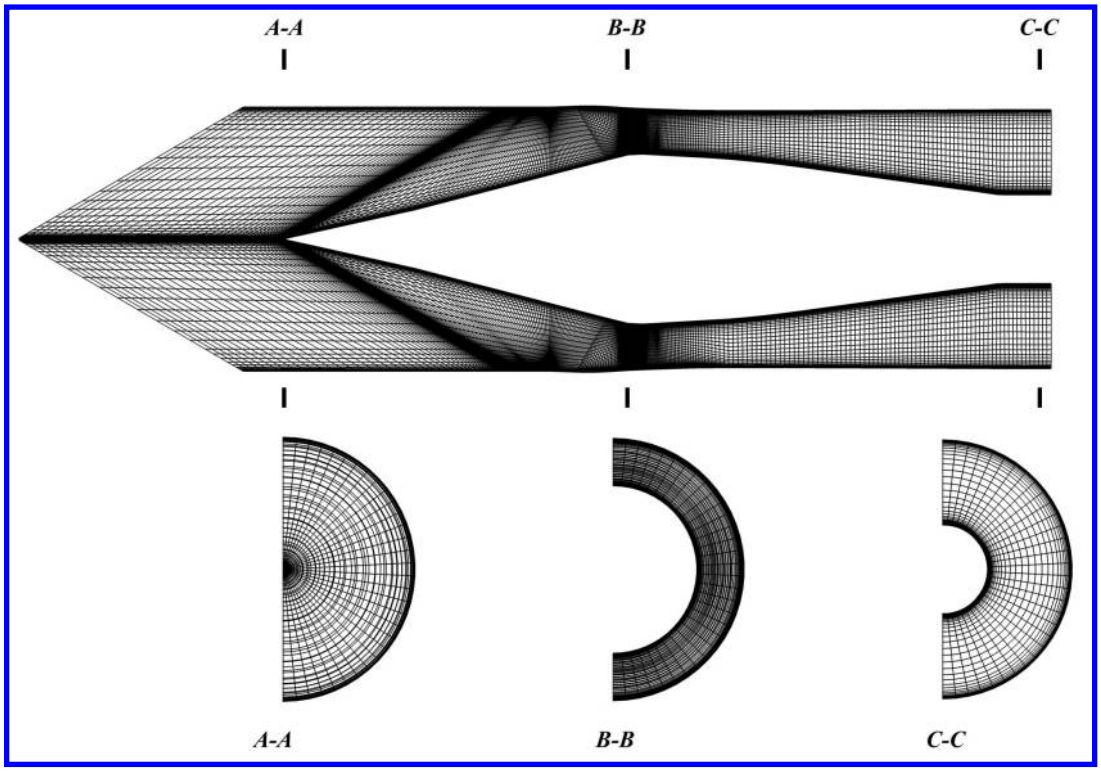

Figure 3: Cutaway views of mesh of the mixed compression inlet at streamwise plane, freestream region($A-A$), throat($B-B$), and the inlet exit($C-C$).

The cowl bleed ducts, vortex generators, overboard bypasses, struts and rakes are ignored in this study. To better resolve the oblique conic shock wave, the freestream mesh is aligned with the Mach cone angle μ as:

$$\mu = asin\frac{1}{Ma_\infty} \tag{5}$$

In this study, Ma_∞=2.0, μ=30°. The freestream flow conditions in the CFD simulation are shown in Table 1.

The Mach number contours of the baseline validation result at $AoA = 0°$ is shown in Fig. 4(a). It can be seen that, at the bleed mass rate of 1.3%, the FASIP flowfield result is very similar to that calculated by Zha *et al*[32](b), and the normal shock over the bleed slot is correctly predicted.

Downloaded by Gecheng Zha on January 3, 2022 | http://arc.aiaa.org | DOI: 10.2514/6.2022-2234

Table 1: Flow Conditions and Model Characteristics

Parameter	Value
M_∞	2.0
Re, based on R_c	1.55×10^6
$P_{t\infty}$	$7.67 \times 10^4 Pa$[32]
$T_{t\infty}$	390K
P_{exit}	$6.29 \times 10^4 Pa$
$\dot{m}_{bleed}/\dot{m}_0$ (Mass Flow Ratio)	1.3%
R_c	0.2365m [36]

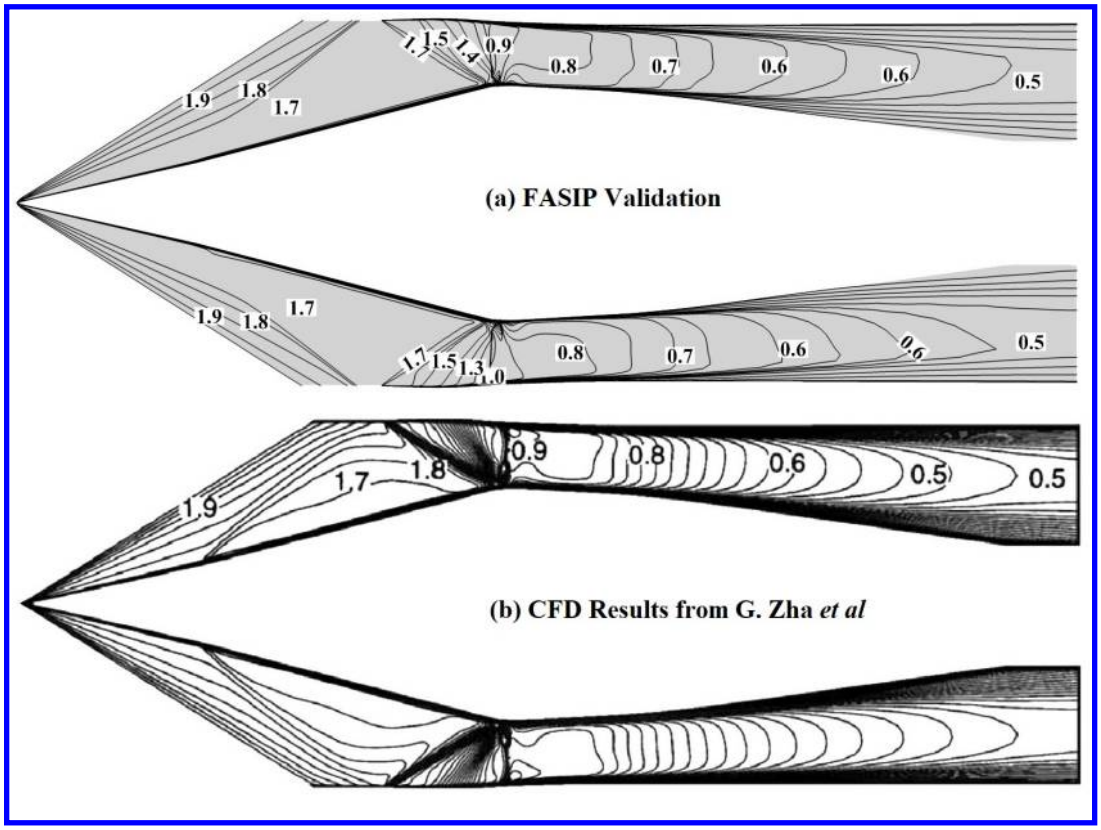

Figure 4: Mach number contour of the inlet at Ma_∞=2.0; FASIP results(a) and CFD simulation results by Zha *et al*[33](b).

A comparison of centerbody pressure distributions $P/P_{t\infty}$ at zero angle of attack and critical operation between the experiment[35] and the present simulation as well as the one from [33], is shown in Fig. 5. The experimental bleed mass rate of 1.3% is used.

Downloaded by Gecheng Zha on January 3, 2022 | http://arc.aiaa.org | DOI: 10.2514/6.2022-2234

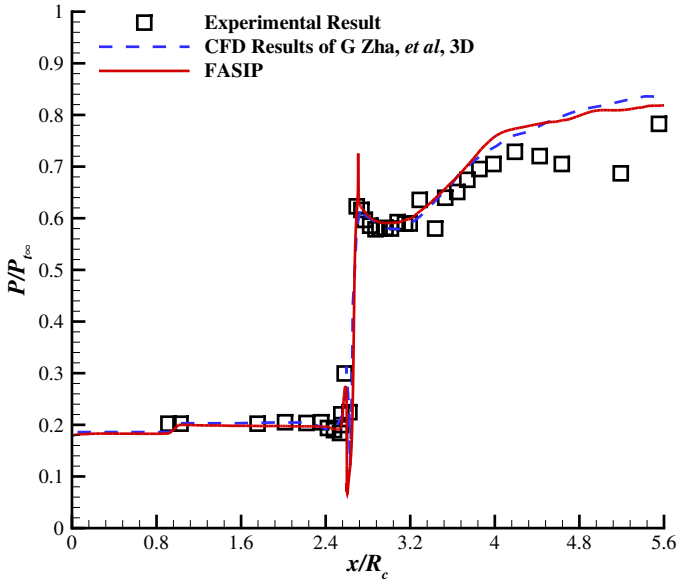

Figure 5: Comparison of Static Pressure Distributions along the Centerbody.

Fig. 5 indicates that the shock position, the external compression due to the cone, and the pressure behind the normal shock in the subsonic diffuser are in very good agreement with the experiment even though the shock strength is a little over-predicted numerically. The discrepancy near the outlet is due to the omitted centerbody struts, which do not affect the inlet stability as observed in the present study and in [33].

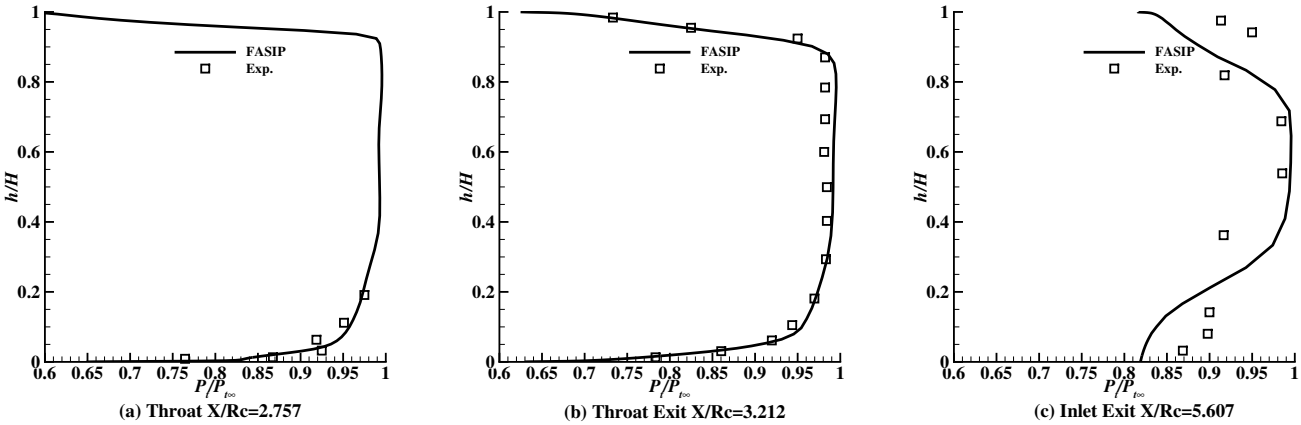

Figure 6: Comparison of Total Pressure Profiles along the Streamwise Direction.

Fig. 6 presents the total pressure profiles at the inlet throat ($X/R_c = 2.757$), throat exit ($X/R_c = 3.212$), and inlet exit or fan face($X/R_c = 5.607$). The predicted total pressure profile agrees excellently with the experiment at the throat and throat exit. The deviation at the outlet is again due to ignoring the strut as reported in [32].

Downloaded by Gecheng Zha on January 3, 2022 | http://arc.aiaa.org | DOI: 10.2514/6.2022-2234

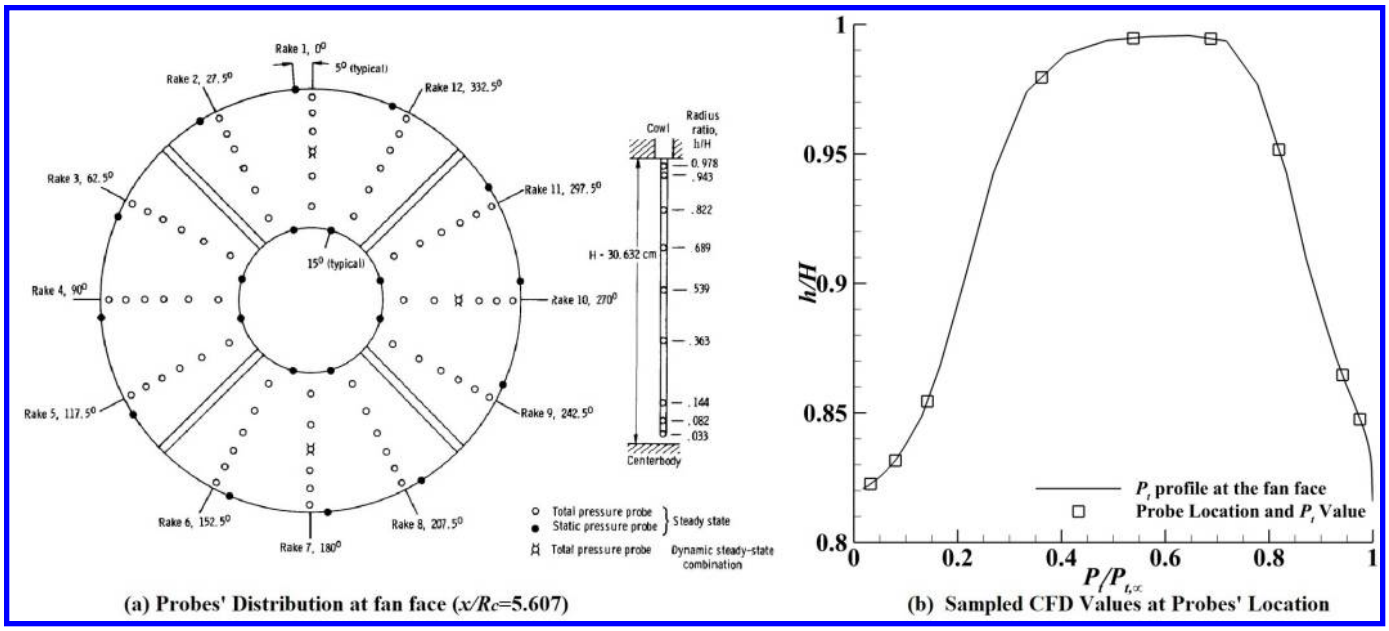

Figure 7: Probe Locations on the Inlet Exit Surface (a) from Wasserbauer *et al* [35] and Corresponding Values on Total Pressure Profile(b).

Fig. 7 shows the circumferential averaged radial distribution of total pressure at the inlet exit. The steady-state distortion is defined as:

$$d_{mass} = \frac{P_{t,max} - P_{t,min}}{\overline{P_t}} \tag{6}$$

The inlet total pressure recovery and distortion based on the experimental probe positions are shown in Table. 2, which indicates that the predicted total pressure recovery is in excellent agreement with the experiment. The predicted inlet distortion, based on the values at experiment probe positions shown in Fig. 7(b), has about 5% deviation from the measurement, which may be attributed to the omitted struts and vortex generators.

Table 2: Inlet Performance Results

Paremeter	FASIP	Zha *et al*[33]	Experiment from [35]
$P_t R_{mass-av}$	0.938	0.939	0.938
$d_{mass-av}$	0.120	0.128	0.114

A validation of baseline inlet unstart angles of attack is conducted, and the Mach number contours on the symmetric planes at different AoAs are shown in Fig. 8:

Downloaded by Gecheng Zha on January 3, 2022 | http://arc.aiaa.org | DOI: 10.2514/6.2022-2234

Downloaded by Gecheng Zha on January 3, 2022 | http://arc.aiaa.org | DOI: 10.2514/6.2022-2234

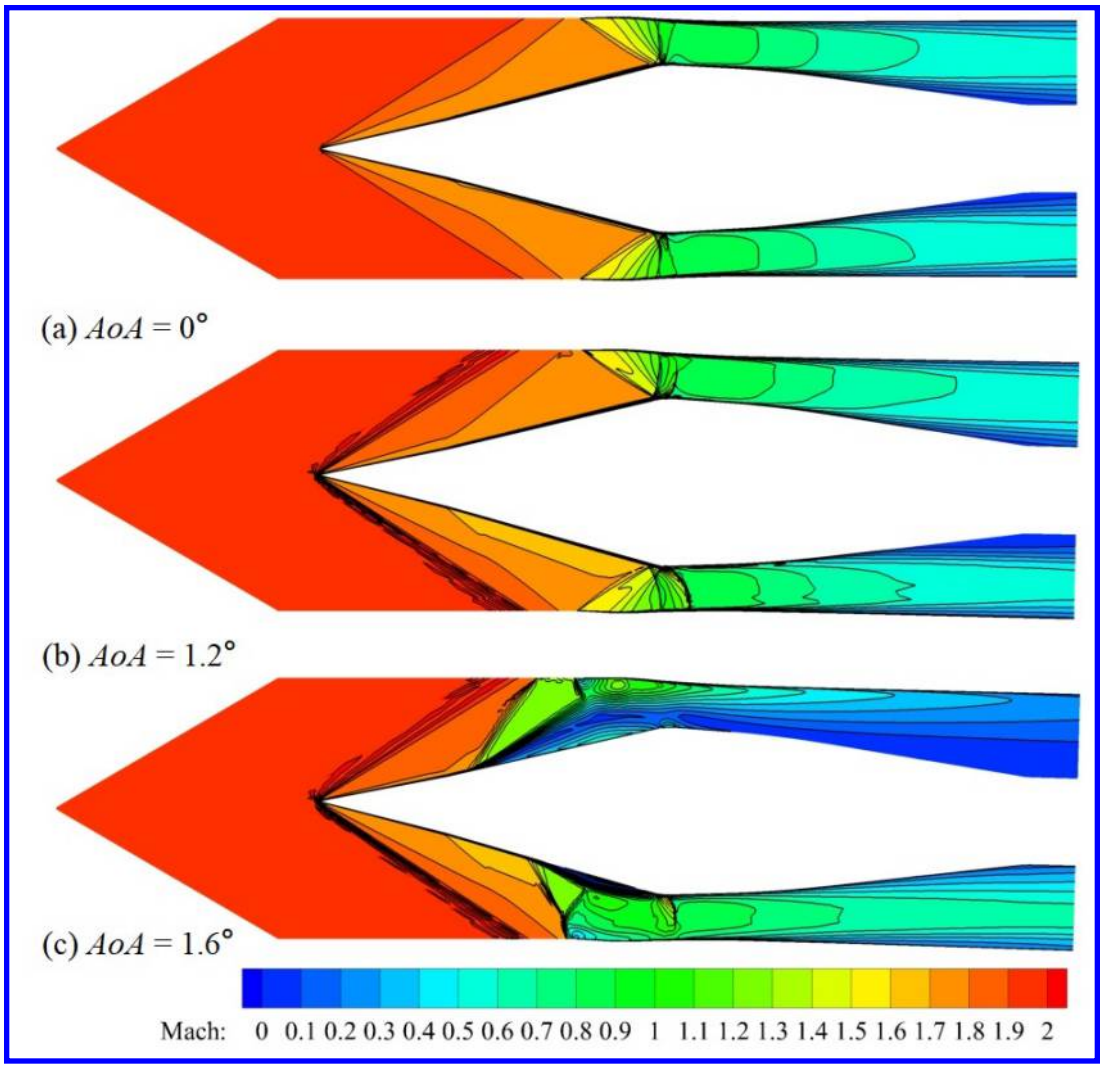

Figure 8: Mach number contours at different AoAs, showing inlet started at $AoA = 0°$ as well as 1.2°, but unstarted at $AoA = 1.6°$.

The baseline inlet remains started at AoA of 1.2° and becomes unstarted at AoA of 1.6°, which is in agreement with the numerical simulation of Zha *et al*[33].

4 CoFlow Jet Inlet

The validated NASA-VDC-Inlet is modified by inserting an CFJ injection slot downstream of the throat in the subsonic diffuser region. The same bleed slot size and location are maintained as the suction slot of the coflow jet. The injection slot is created by slightly contouring the local wall in the diffuser region, but the duct geometry upstream and downstream of the injection slot remains the same to have a fair comparison with the baseline inlet. Fig. 9 shows the suction (blue) and injection slot (red) location of the CFJ-Inlet. The bleed mass flow is fully re-injected into the inlet through this injection slot downstream, thus ZNMF is achieved. The dimensions of the injection slot on the centerbody are shown in Fig. 10. This CFJ injection slot size is designed to handle a maximum mass flow ratio MFR of 1.26%, otherwise the injection slot will be choked.

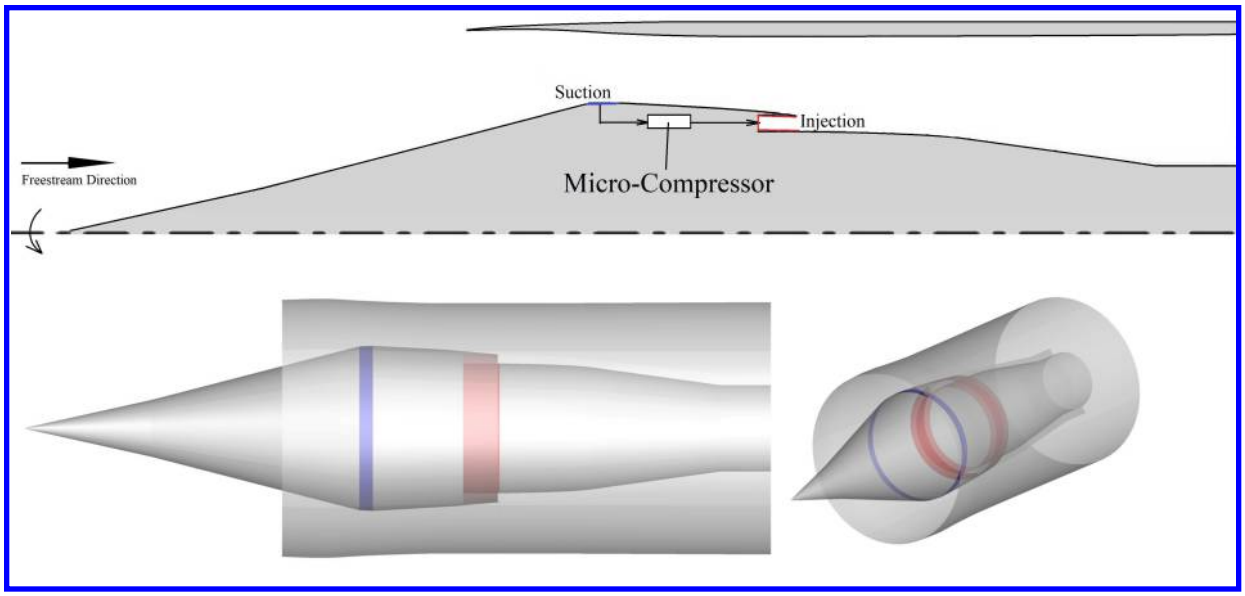

Figure 9: A brief sketch of CFJ Axis Symmetric Supersonic Inlet.

Downloaded by Gecheng Zha on January 3, 2022 | http://arc.aiaa.org | DOI: 10.2514/6.2022-2234

4.1 Principle of CFJ Inlet

The CFJ supersonic inlet flow control has a substantial difference from the subsonic CFJ airfoil flow control. The CFJ inlet withdraws the boundary layer in the throat region and injects the mass flow into the inlet diffuser area downstream. The subsonic CFJ airfoil, as shown in Fig. 1, withdraws the boundary layer downstream near trailing edge and injects the flow upstream near leading edge. Thus, the CFJ inlet and CFJ airfoil flows through the actuators have opposite directions. In other words, the CFJ-inlet-actuated flow has the same direction as the main flow in the inlet, whereas the CFJ-airfoil-actuated flow has an opposite direction to the main flow.

The reasons for such a difference are caused by the difference of Mach number regime and the nature of flow control. First, for the supersonic inlet, withdrawing the mass flow at the throat is proved to be effective by the conventional bleed because the boundary layer is very thick there due to the shock boundary layer interaction. Second, flow-injection to energize nearby flow is effective in subsonic flow area in adverse pressure gradients[37]. This requires the injection to be located in the subsonic diffuser part of the inlet, which must be downstream of the throat as illustrated in Fig. 9 and 10. Based on streamwise pressure distribution shown in Fig. 5, the adverse pressure gradient starts at about x/Rc=3.7, which is hence a desirable location for the injection.

The compound effect of CFJ inlet is that the upstream suction plays the same role as conventional bleed. The downstream injection further energizes the boundary layer and opens up the flow passage, which increases the inlet flow passing capacity and the stability margin even though the diffuser part of the inlet has more flow with the same area.

The power required by the CFJ inlet according to Eq. 3 is determined by the bleed mass flow rate and the ratio of the total pressure between the injection slot and the suction slot. Overall, the total pressure at the bleed slot may be slightly higher than the downstream total pressure at the injection slot. This does not mean that sufficient flow will go from the bleed slot to the injection slot by itself as a passive flow control. In reality, the flow path from the suction to the downstream injection will suffer total pressure loss. The flow from the upstream suction usually will not have sufficient energy to generate the required injection momentum downstream. Thus, a compressor actuator between the suction slot and the injection slot as sketched in Fig. 9 is needed. However, the

flow path with minimal total pressure loss can be designed to minimize the power required for the fluidic actuators as done in [38, 39, 40], which is a topic beyond the scope of this paper. What we want to prove in this paper is that the concept of the CFJ flow control is feasible to stabilize the supersonic inlet with constant mass flow rate to benefit the overall system. The detailed design of the CFJ flow path will be left as a future work.

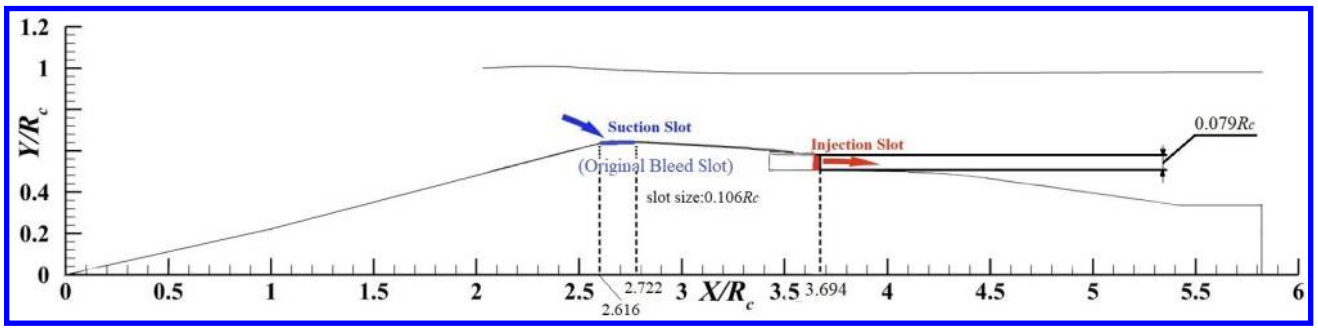

Figure 10: Dimensions and shape of the CFJ-Inlet geometry.

5 Results and Discussion

The CFJ simulations are performed with the freestream condition of Ma=2.0, Re = 1.55×10^6 (based on R_c=0.2365m).

5.1 CFJ Effects on Flows at Critical Conditions

This section examines the inlet flows affected by the energy transfer process of the ZNMF CFJ flow control when the inlets remain started. Fig. 11 shows the Mach number contour of CFJ-Inlet at AoA=0°, CFJ MFR = 1.26%. It can be seen that the flow at the injection duct exit is choked. If more flow is to be injected, the injection slot needs to be enlarged. The injection jet energizes the boundary layer in the diffuser portion on the centerbody. In the suction (bleed) slot as shown in the zoomed plot of Fig. 11, a normal shock occurs in the aft portion of the slot as desired. A normal shock emanating from the cowl wall appears upstream of the terminal normal shock standing above the bleed slot. A small low-speed flow region is formed right after the slot due to the high pressure gradient caused by the shock wave. The boundary layer upstream of the suction slot on the centerbody is eliminated by the bleed flow. This establishes the required flow condition to stabilize the inlet at the critical condition, even though bleed mass flow is 5% less than that of the baseline inlet and is put back to the inlet downstream.

Another simulation is conducted to reduce the CFJ bleed mass flow to MFR=0.7%, a reduction of 46% of the baseline bleed mass flow. Fig. 12 shows the Mach number contour of CFJ-Inlet at AoA=0°, CFJ MFR = 0.7%, which shows that the inlet remains started at critical condition. At this reduced bleed flow condition, the normal shock from the cowl wall shown in Fig. 11 with the higher suction mass flow rate disappears. Multiple shock waves system at the throat is more stable and has less energy loss than a single terminal shock. The Mach number at the injection slot exit is only about 0.4 due to reduced mass flow rate. The boundary layer in the diffuser downstream of the injection is energized too, but not as much as that shown in Fig. 11. The boundary layer upstream of the bleed slot is still well eliminated by the CFJ suction. When the jet mass flow ratio is further reduced to 0.56%, the inlet becomes unstarted, as shown in Fig. 13.

Downloaded by Gecheng Zha on January 3, 2022 | http://arc.aiaa.org | DOI: 10.2514/6.2022-2234

Downloaded by Gecheng Zha on January 3, 2022 | http://arc.aiaa.org | DOI: 10.2514/6.2022-2234

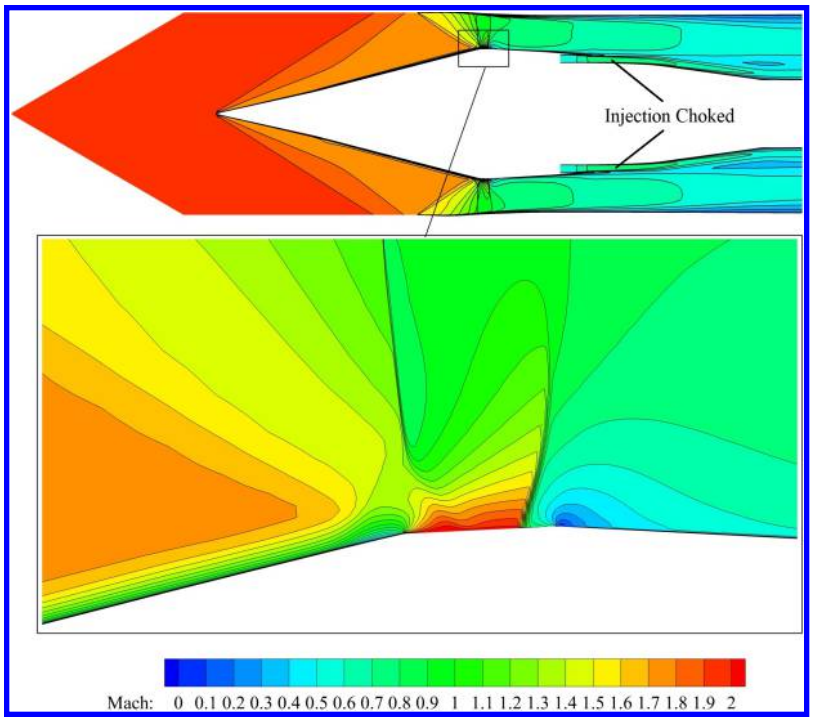

Figure 11: Mach number contour of CFJ-Inlet at symmetric plane, $AoA = 0°$, CFJ mass flow rate = 1.26% of the captured mass flow rate.

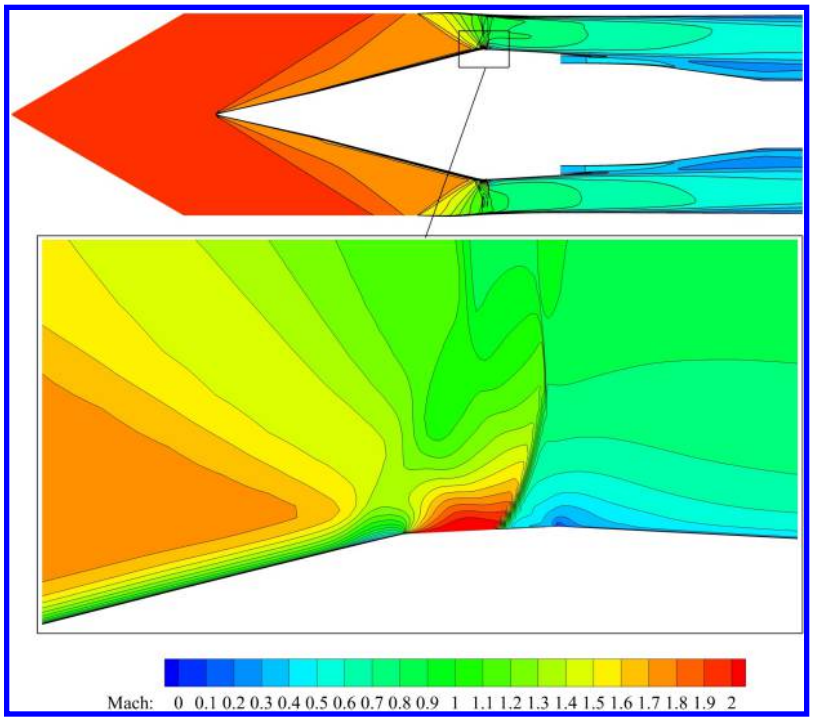

Figure 12: Mach number contour of CFJ-Inlet at symmetric plane, $AoA = 0°$, CFJ mass flow rate = 0.7% of the captured mass flow rate.

Downloaded by Gecheng Zha on January 3, 2022 | http://arc.aiaa.org | DOI: 10.2514/6.2022-2234

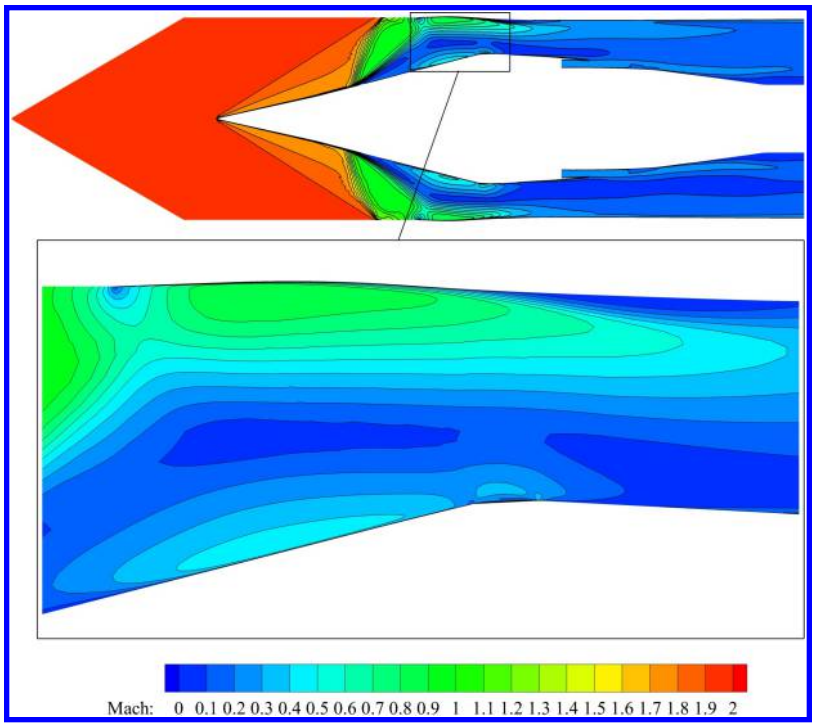

Figure 13: Mach number contour of CFJ-Inlet at symmetric plane, $AoA = 0°$, CFJ mass flow rate = 0.56% of the captured mass flow rate. The inlet is unstarted.

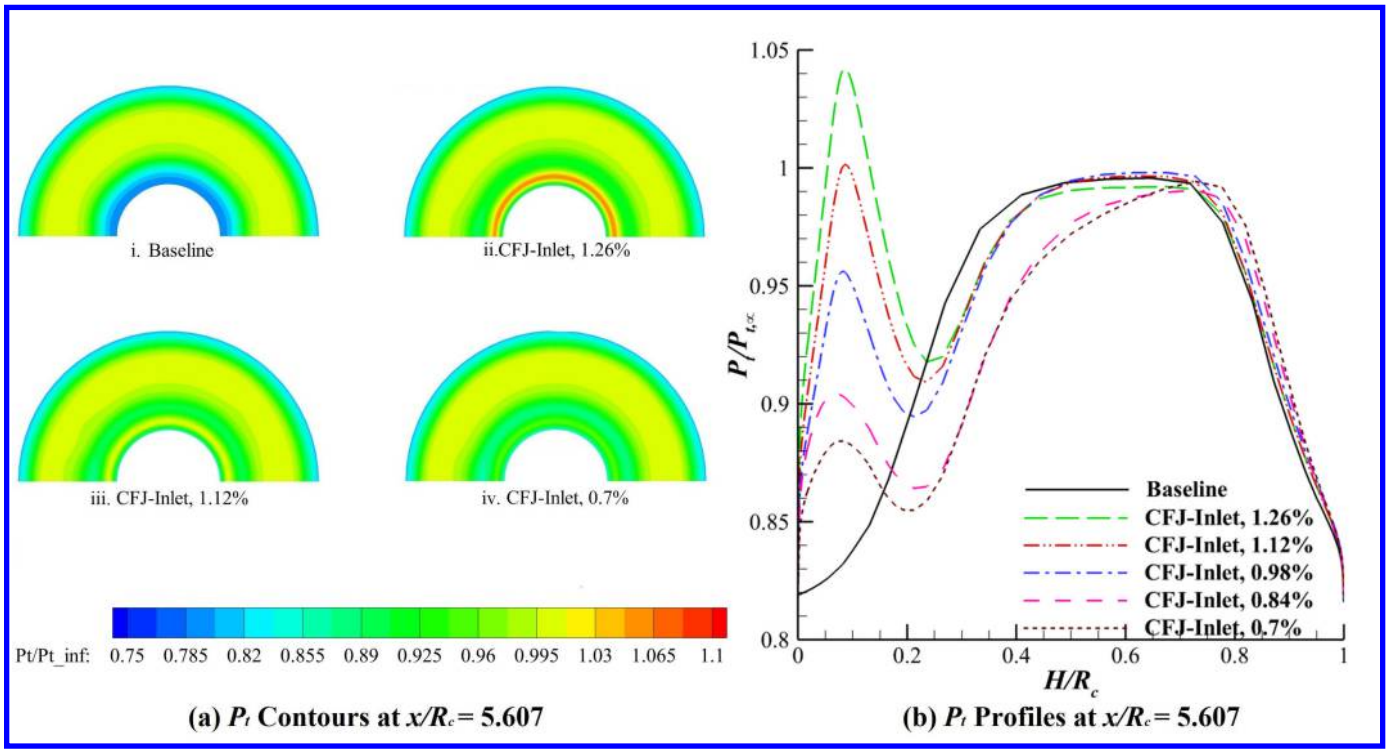

Figure 14: Results of baseline and CFJ-Inlet with varied CFJ mass flow ratios, in total pressure contours(a) and normalized total pressure profile at inlet exit(b).

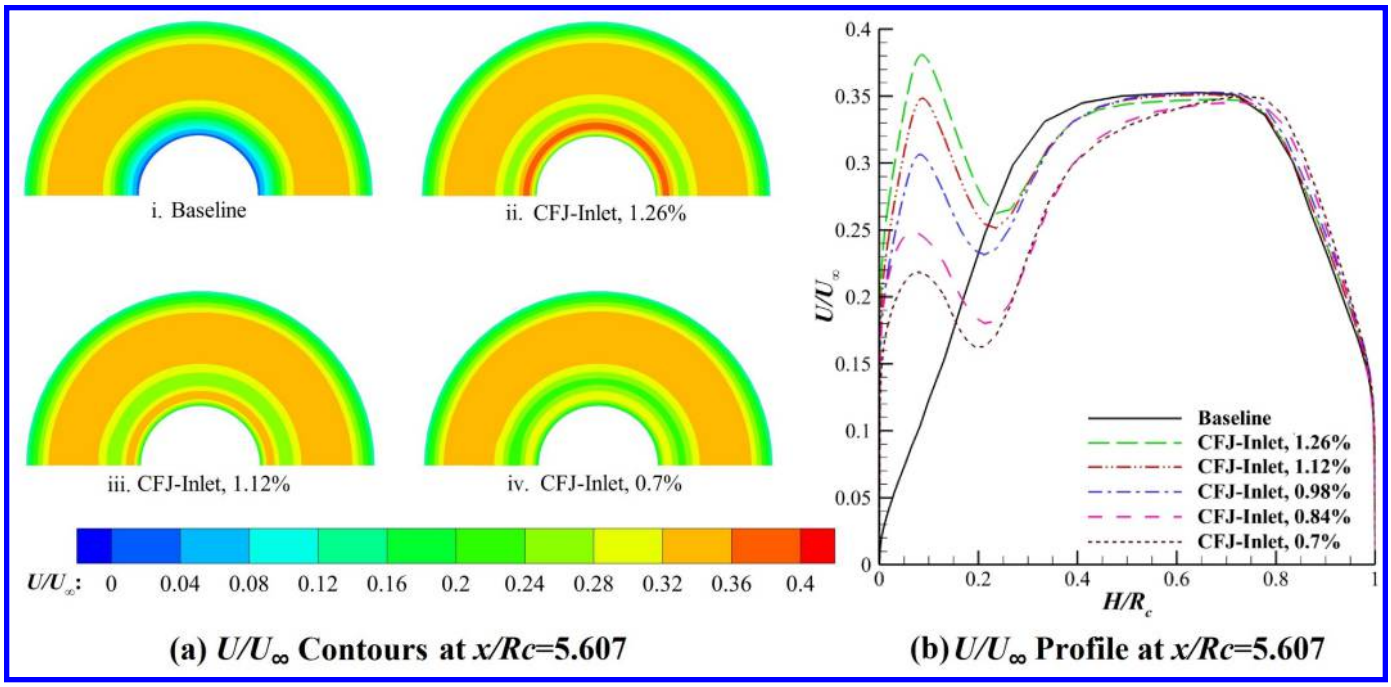

Figure 15: Results of baseline and CFJ-Inlet with varied CFJ mass flow ratios, in normalized axial velocity(a) and its profile at inlet exit(b).

To study the mass flow rate effect affecting the inlet performance including the stability and total pressure recovery, five CFJ mass flow ratios that can maintain the inlet started, 1.26%, 1.12%, 0.98%, 0.84% and 0.7%, are simulated. Fig. 14(a) and Fig. 15(a)shows the contours of normalized total pressure and axial velocity respectively at the inlet exit (x/R_c=5.607), whereas Fig. 14(b) and and Fig. 15(b) shows the normalized total pressure profiles and axial velocity respectively along the radial span.

Fig. 14 (a) and (b) clearly show that the total pressure on the center body at the inlet exit is substantially higher than that of the baseline inlet with no flow control even though all of those flows are at critical conditions. Similar to Fig. 14, Fig. 15 plots the axial velocity contours, Fig. 15(a), and its radial profiles, Fig. 15, based on circumferential average. As expected, the velocity profiles of the CFJ inlet near the centerbody are substantially higher than that of the baseline due to the CFJ injection. The injection reduces the flow blockage caused by the low momentum flow in the diffuser region and increases the flow capacity, which increase the inlet stability, total pressure recovery, and system efficiency.

Table 3: Performances and Power Characteristics of Varied Started Cases

Inlet	mass flow	$P_{t,inj}/P_{t,suc}$	P_tR	P_tR increase	C_μ	$d_{mass-av}$
Baseline	1.3%	-	0.938	-	0	0.185
CFJ	1.26%	0.707	0.955	1.81%	0.080	0.234
CFJ	1.12%	0.648	0.961	2.45%	0.061	0.193
CFJ	0.98%	0.609	0.949	1.17%	0.054	0.191
CFJ	0.84%	0.558	0.932	-0.06%	0.040	0.184
CFJ	0.70%	0.597	0.928	-1.01%	0.028	0.190

Table 3 shows the performance parameters comparing the CFJ inlet with the baseline inlet for all the started

Downloaded by Gecheng Zha on January 3, 2022 | http://arc.aiaa.org | DOI: 10.2514/6.2022-2234

inlet cases with varied mass flow ratios, including the CFJ mass flow ratio(MFR), total pressure ratio between injection slot and suction slot, total pressure recovery of the inlet, injection jet momentum coefficient, and engine interface distortion. All the CFJ inlet has lower suction (bleed) MFR than the baseline inlet and still achieve the critical condition. Because we omit the flow path between the bleed suction slot and the injection slot, all the total pressures at the suction slot are higher than that of the injection slot. Thus the total pressure ratio between the injection and suction are less than 1 and decreases when the mass flow rate is reduced. Because the total pressure ratio is less than 1, the power required by CFJ would be negative. It means that the flow can go by itself from the bleed suction slot to the injection. In reality, the total pressure loss in the flow path is believed to require a power to pump the flow depending on the specific flow path design.

For the CFJ inlet with the MFR between 0.98% and 1.26%, the total pressure recovery is higher than the baseline inlet. For the two lower MFRs of 0.84% and 0.70%, the inlet total pressure recovery is actually lower than the baseline model. This is because when the bleed MFR is low such as 0.7%, the terminal shock becomes stronger and creates more total pressure loss as explained for Fig. 12. That is why when the suction MFR is too low such as at 0.56% as the case in Fig. 13, the terminal normal shock becomes too strong and will propagate to upstream and brings the inlet to unstart. The CFJ inlet distortion is higher than that of the baseline inlet when the CFJ MFR is high. This is because of the high total pressure energized locally as shown in Fig. 14. At the lower CFJ mass flow ratio, the distortion is about the same as the baseline.

Downloaded by Gecheng Zha on January 3, 2022 | http://arc.aiaa.org | DOI: 10.2514/6.2022-2234

5.2 Unstart Margin of CFJ Inlet due to Angle of Attack

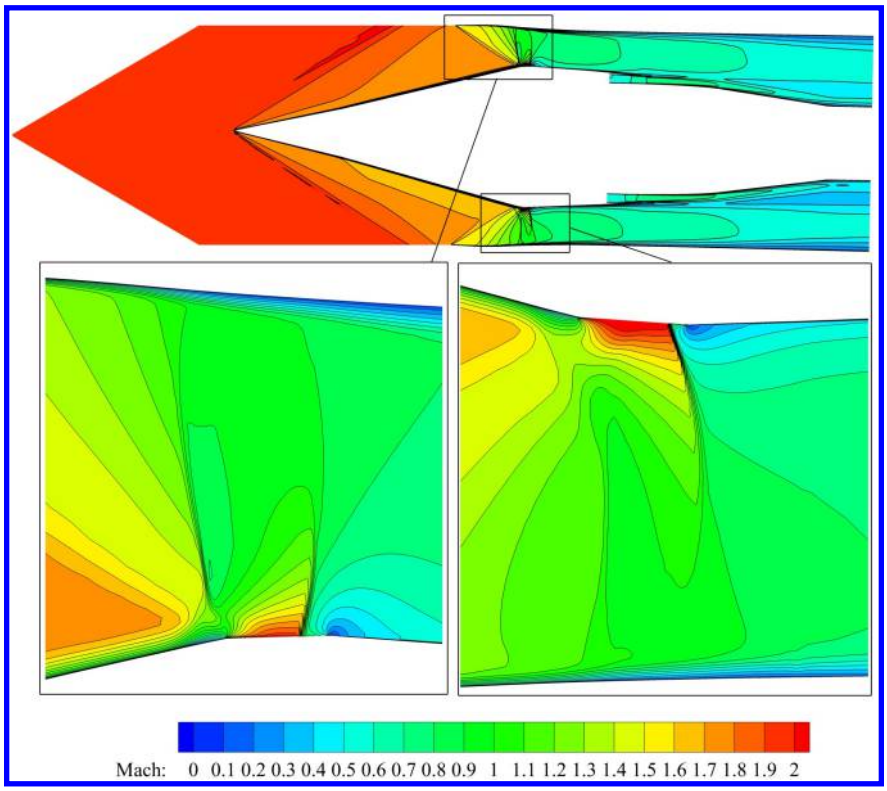

Figure 16: Mach number contour of CFJ-Inlet at symmetric plane, $AoA = 1.2°$, CFJ mass flow rate = 1.26% of the captured mass flow rate.

Fig. 16 shows the Mach number contour of CFJ-Inlet at AoA=1.2°, CFJ MFR = 1.26%. It shows that, the inlet remains at critical condition. The overall flow strictures are very much the same as those at AoA of 0° shown in Fig. 11. When the CFJ MFR is reduced to 0.98%, the inlet still remains started as shown in Fig. 17. With the CFJ mass flow ratio of 1.26% and the AoA of 2.0°, which is beyond the baseline inlet unstart AoA of 1.6°, the inlet remains started. The flowfields of the CFJ-Inlet at AoA = 1.6° and 2.0° are shown in Fig. 18.

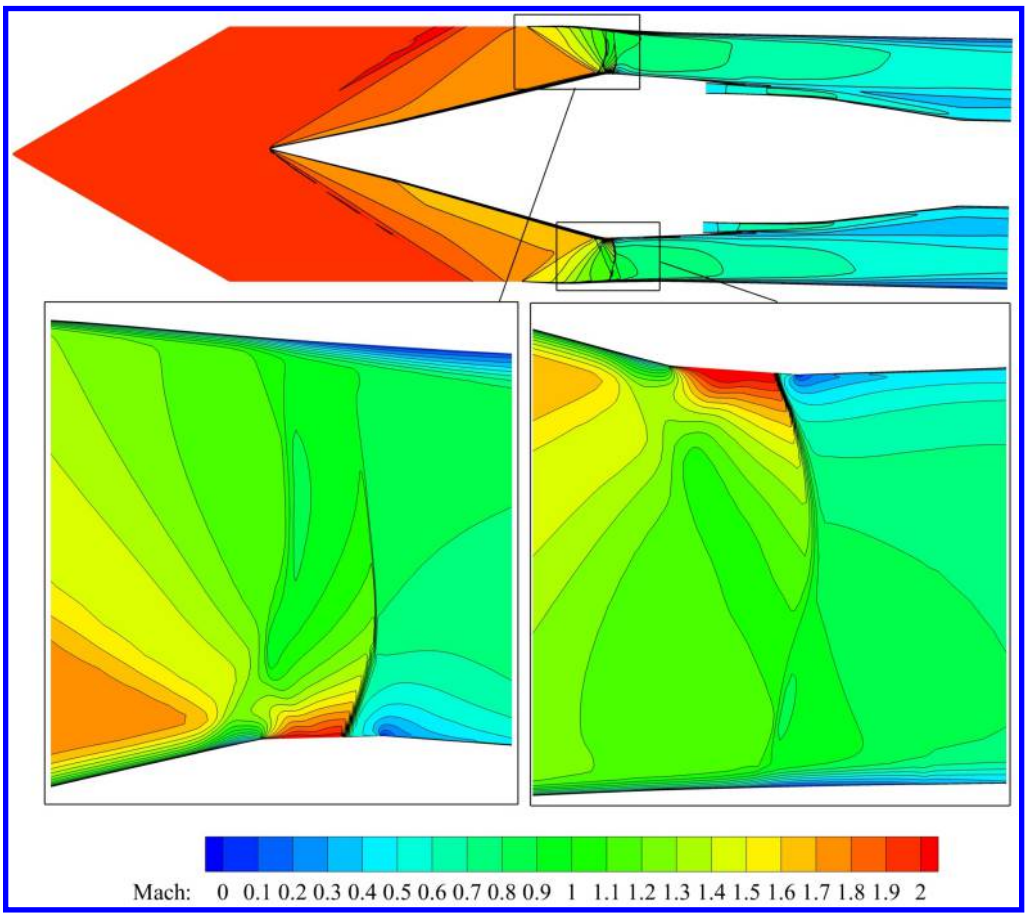

Figure 17: Mach number contour of CFJ-Inlet at symmetric plane, AoA = 1.2°, CFJ mass flow rate = 0.98% of the captured mass flow rate.

This result indicates that the CFJ inlet is able to bleed less amount of flow with zero-net-mass-flux control and achieves even higher inlet stability. At AoA = 2.8°, MFR = 1.26% the inlet is unstarted as shown in Fig. 19. More detailed studies are in progress to find the maximum AoA.

Downloaded by Gecheng Zha on January 3, 2022 | http://arc.aiaa.org | DOI: 10.2514/6.2022-2234

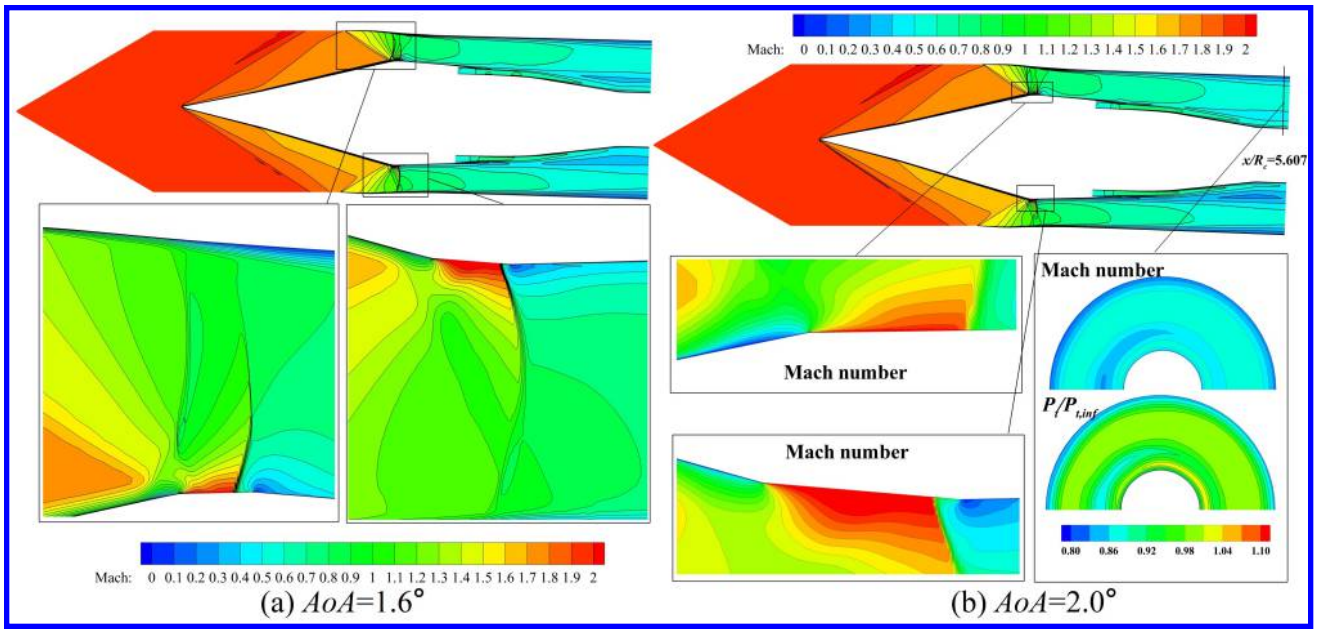

Figure 18: Mach number contours of CFJ-Inlet at symmetric plane, $AoA = 1.6°$(a) and $AoA = 2.0°$(b), both with CFJ mass flow ratio = 1.26%.

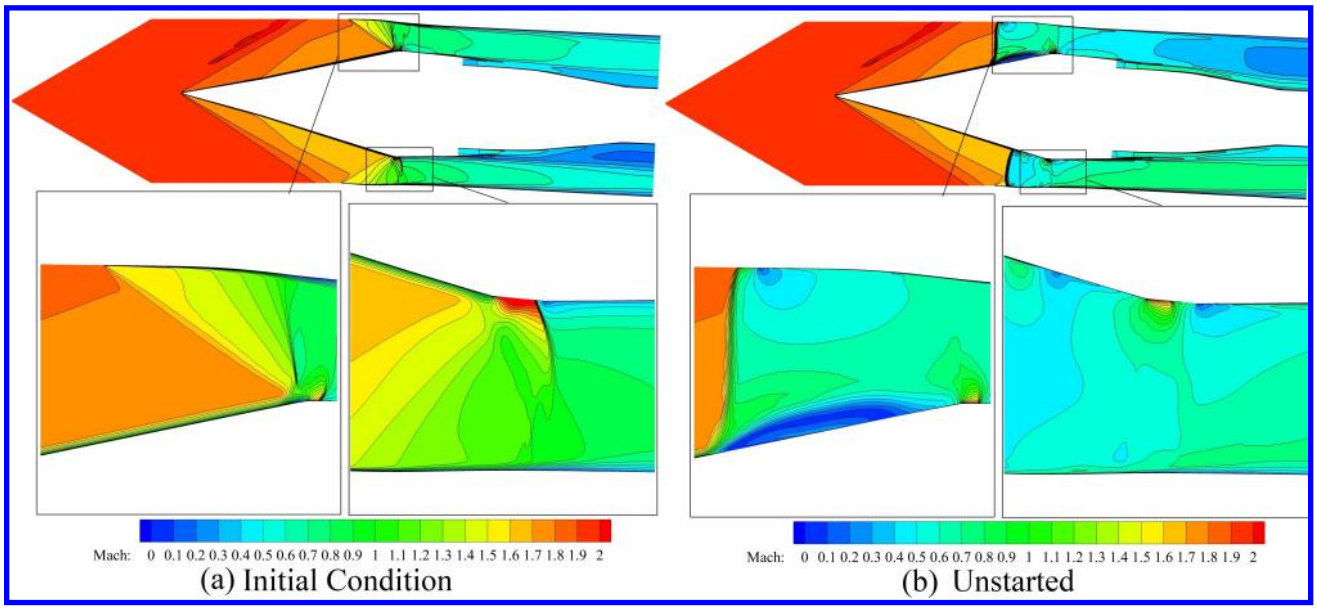

Figure 19: Mach number contour of CFJ-Inlet at symmetric plane, $AoA = 2.8°$, CFJ mass flow rate = 1.26% of the captured mass flow rate.

6 Conclusions

The validated numerical study demonstrates that for axis-symmetric mixed-compression supersonic inlet: 1) CoFlow jet flow control appears feasible to withdraw the bleed flow at the inlet throat and inject it back to the inlet downstream in the subsonic diffuser region to achieve constant mass flow throughout the inlet. 2) CFJ inlet

Downloaded by Gecheng Zha on January 3, 2022 | http://arc.aiaa.org | DOI: 10.2514/6.2022-2234

is able to substantially reduce the bleed mass flow while still maintains the inlet stability and increase efficiency. 3) The mechanism of CFJ inlet to stabilize axis-symmetric inlet is two-fold: i) The suction in the bleed region has the same effect as conventional bleed to remove the thick boundary layer in the throat region. ii) The downstream injection further enhances the effect by energizing the boundary layer in the diffuser region to reduce flow blockage, increase flow passing capacity, and thus achieve higher inlet stability, inlet efficiency and system efficiency. The CFD simulation indicates that the baseline inlet remains started at AoA of 1.2°, and unstarts at AoA of 1.6°. With a 5% less bleed mass flow than that of the baseline inlet, the CFJ inlet is able to stabilize the inlet at AoA of 2.0° with higher total pressure recovery, while keeping the constant mass flow in the inlet. More numerical studies to investigate the working mechanism of CFJ inlets are in progress.

7 Acknowledgment

The simulations are conducted on Pegasus super-computing system at the Center for Computational Sciences (CCS) at the University of Miami.

Disclosure: The University of Miami and Dr. Gecheng Zha may receive royalties for future commercialization of the intellectual property used in this study. The University of Miami is also equity owner in CoFlow Jet, LLC, licensee of the intellectual property used in this study.

Downloaded by Gecheng Zha on January 3, 2022 | http://arc.aiaa.org | DOI: 10.2514/6.2022-2234

References

[1] Y. Sun and H. Smith, "Review and prospect of supersonic business jet design," *Progress in Aerospace Sciences*, vol. 90, pp. 12–38, 2017.

[2] R. Hutchinson, J. Lawrence, and K. F. Joiner, "Conceptual design and integration of a propulsion system for a supersonic transport aircraft," *Proceedings of the Institution of Mechanical Engineers, Part G: Journal of Aerospace Engineering*, p. 09544100211016952, 2021.

[3] J. Morgenstern, N. Norstrud, J. Sokhey, S. Martens, and J. J. Alonso, *Advanced Concept Studies for Supersonic Commercial Transports Entering Service in the 2018 to 2020 Period:.* National Aeronautics and Space Administration, Glenn Research Center, 2013.

[4] G.-C. Zha and D. C. Paxton, "A Novel Flow Control Method for Airfoil Performance Enhancement Using Co-Flow Jet." *Applications of Circulation Control Technologies*, Chapter 10, p. 293-314, Vol. 214, Progress in Astronautics and Aeronautics, AIAA Book Series, Editors: Joslin, R. D. and Jones, G.S., 2006.

[5] G.-C. Zha, W. Gao, and C. Paxton, "Jet Effects on Co-Flow Jet Airfoil Performance," *AIAA Journal, No. 6,*, vol. 45, pp. 1222–1231, 2007.

[6] G.-C. Zha, C. Paxton, A. Conley, A. Wells, and B. Carroll, "Effect of Injection Slot Size on High Performance Co-Flow Jet Airfoil," *AIAA Journal of Aircraft*, vol. 43, 2006.

[7] G.-C. Zha, B. Carroll, C. Paxton, A. Conley, and A. Wells, "High Performance Airfoil with Co-Flow Jet Flow Control," *AIAA Journal*, vol. 45, 2007.

[8] Wang, B.-Y. and Haddoukessouni, B. and Levy, J. and Zha, G.-C., "Numerical Investigations of Injection Slot Size Effect on the Performance of Co-Flow Jet Airfoil," *Journal of Aircraft*, vol. Vol. 45, No. 6,, pp. pp.2084–2091, 2008.

[9] B. P. E. Dano, D. Kirk, and G.-C. Zha, "Experimental Investigation of Jet Mixing Mechanism of Co- Flow Jet Airfoil." AIAA-2010-4421, 5th AIAA Flow Control Conference, Chicago, IL, 28 Jun - 1 Jul 2010.

[10] B. Dano, G. Zha, and M. Castillo, "Experimental study of co-flow jet airfoil performance enhancement using discreet jets," in *49th AIAA Aerospace Sciences Meeting including the New Horizons Forum and Aerospace Exposition*, p. 941, 2011.

[11] A. Lefebvre, B. Dano, W. Bartow, M. Fronzo, and G. Zha, "Performance and energy expenditure of coflow jet airfoil with variation of mach number," *Journal of Aircraft*, vol. 53, no. 6, pp. 1757–1767, 2016.

[12] A. Lefebvre, G-C. Zha, "Numerical Simulation of Pitching Airfoil Performance Enhancement Using Co-Flow Jet Flow Control," *AIAA paper 2013-2517*, June 2013.

[13] A. Lefebvre, G-C. Zha, "Cow-Flow Jet Airfoil Trade Study Part I : Energy Consumption and Aerodynamic Performance," *32nd AIAA Applied Aerodynamics Conference, AIAA AVIATION Forum, AIAA 2014-2682*, June 2014.

[14] A. Lefebvre, G-C. Zha, "Cow-Flow Jet Airfoil Trade Study Part II : Moment and Drag," *32nd AIAA Applied Aerodynamics Conference, AIAA AVIATION Forum, AIAA 2014-2683*, June 2014.

[15] Lefebvre, A. and Zha, G.-C., "Trade Study of 3D Co-Flow Jet Wing for Cruise Performance." AIAA Paper 2016-0570, AIAA SCITECH2016, AIAA Aerospace Science Meeting, San Diego, CA, 4-8 January 2016.

[16] G.-C. Zha, Y. Shen, and B. Wang, "An improved low diffusion E-CUSP upwind scheme ," *Journal of Computer & Fluids*, vol. 48, pp. 214–220, 2011.

[17] Shen, Y.Q., and Zha, G.C., "Large Eddy Simulation Using a New Set of Sixth Order Schemes for Compressible Viscous Terms," *Journal of Computational Physics*, vol. 229, pp. 8296–8312, doi:10.1016/j.jcp.2010.07.017, 2010.

[18] Shen, Y.-Q. and Zha, G.-C. and Chen, X.-Y., " High Order Conservative Differencing for Viscous Terms and the Application to Vortex-Induced Vibration Flows," *Journal of Computational Physics*, vol. 228(2), pp. 8283–8300, 2009.

[19] Shen, Y.-Q. and Zha, G.-C. , " Improvement of the WENO Scheme Smoothness Estimator," *International Journal for Numerical Methods in Fluids*, vol. DOI:10.1002/fld.2186, 2009.

[20] G.-C. Zha and E. Bilgen, "Numerical study of three-dimensional flows using unfactored upwind-relaxation sweeping algorithm," *Journal of Computational Physics*, vol. 125, no. 2, pp. 425–433, 1996.

[21] Y.-Q. Shen, G.-C. Zha, and B.-Y. Wang, "Improvement of Stability and Accuracy of Implicit WENO Scheme ," *AIAA Journal*, vol. 47, pp. 331–344, 2009.

[22] G.-C. Zha and E. Bilgen, "Numerical Solutions of Euler Equations by Using a New Flux Vector Splitting Scheme ," *International Journal for Numerical Methods in Fluids*, vol. 17, pp. 115–144, 1993.

[23] X.-Y. Chen and G.-C. Zha, "Fully Coupled Fluid-Structural Interactions Using an Efficient High Solution Upwind Scheme." AIAA Paper 2004-2331, to appear in Journal of Fluids and Structures, 2005.

[24] B.-Y. Wang and G.-C. Zha, "A General Sub-Domain Boundary Mapping Procedure For Structured Grid CFD Parallel Computation," *AIAA Journal of Aerospace Computing, Information, and Communication*, vol. 5, No.11, pp. 2084–2091, 2008.

Downloaded by Gecheng Zha on January 3, 2022 | http://arc.aiaa.org | DOI: 10.2514/6.2022-2234

[25] Lefebvre, A. and Dano, B. and Bartow, W. and Di Franzo, M. and Zha, G.-C., "Performance and Energy Expenditure of Coflow Jet Airfoil with Variation of Mach Number." AIAA Paper 2013-0490, AIAA Journal of Aircraft, DOI: 10.2514/1.C033113, 2016.

[26] Y. Yang and G. Zha, "Super-lift coefficient of active flow control airfoil: What is the limit?," in *55th AIAA Aerospace Sciences Meeting*, p. 1693, 2017.

[27] K. Xu and G. Zha, "High control authority three-dimensional aircraft control surfaces using coflow jet," *Journal of Aircraft*, vol. 58, no. 1, pp. 72–84, 2021.

[28] G. Zha, W. Gao, and C.D. Paxton, "Jet Effects on Co-Flow Jet Airfoil Performance," *AIAA Journal*, vol. 45, pp. 1222–1231, 2007.

[29] B. Dano, G. Zha, and M. Castillo, "Experimental study of co-flow jet airfoil performance enhancement using discreet jets." AIAA Paper 2011-941, 49th AIAA Aerospace Sciences Meeting including the New Horizons Forum and Aerospace Exposition, Orlando, Florida, 04 January 2011 - 07 January 2011.

[30] Liu, Z.-X. and Zha, G.-C., "Transonic Airfoil Performance Enhancement Using Co-Flow Jet Active Flow Control." AIAA Paper 2016-3066, AIAA Aviation, Washington, D.C., June 13-17 2016.

[31] Lefebvre, A. and Zha, G.-C. , "Design of High Wing Loading Compact Electric Airplane Utilizing Co-Flow Jet Flow Control." AIAA Paper 2015-0772, AIAA SciTech2015: 53nd Aerospace Sciences Meeting, Kissimmee, FL, 5-9 Jan 2015.

[32] G.-C. Zha, D. Knight, D. Smith, and M. Haas, "Numerical simulation of high-speed civil transport inlet operability with angle of attack," *AIAA journal*, vol. 36, no. 7, pp. 1223–1229, 1998.

[33] G.-C. Zha, D. Knight, and D. Smith, "Investigations of high-speed civil transport inlet unstart at angle of attack," *Journal of aircraft*, vol. 35, no. 6, pp. 851–856, 1998.

[34] J. F. Wasserbauer, H. E. Neumann, and R. J. Shaw, "Distortion in a full-scale bicone inlet with internal focused compression and 45 percent internal contraction," 1974.

[35] J. F. Wasserbauer, R. J. Shaw, and H. E. Neumann, "Design of a very-low-bleed mach 2.5 mixed-compression inlet with 45 percent internal contraction," tech. rep., 1975.

[36] D. A. Choby and J. Wasserbauer, "Mach 2.5 performance of a bicone inlet with internal focused compression and 40 percent internal contraction," tech. rep., 1971.

[37] K. Xu, Y. Ren, and G. Zha, "Separation control by co-flow wall jet," in *AIAA AVIATION 2021 FORUM*, p. 2946, 2021.

[38] Y. Ren and G. Zha, "Design of injection and suction ducts for co-flow jet airfoils with embedded micro-compressor actuator," in *2018 Flow Control Conference*, p. 3062, 2018.

[39] Y. Ren and G. Zha, "Design of injection jet span profile for co-flow jet airfoil," in *AIAA Scitech 2019 Forum*, p. 0589, 2019.

[40] P. A. Barrios, Y. Ren, K. Xu, and G. Zha, "Design of 3d co-flow jet airfoil with integrated micro-compressor for high operating efficiency at cruise condition," in *AIAA AVIATION 2021 FORUM*, p. 2581, 2021.

Downloaded by Gecheng Zha on January 3, 2022 | http://arc.aiaa.org | DOI: 10.2514/6.2022-2234